JOURNAL OF Materials CHEMISTRY

Crystal structure of monophosphate tungsten bronze $K_{1.33}P_4W_8O_{32}$ at 110 K

Michal Dusek,[a,b] Jens Lüdecke[a] and Sander van Smaalen*[a]

[a]*Laboratory of Crystallography, University of Bayreuth, D-95440 Bayreuth, Germany. E-mail: smash@uni-bayreuth.de*
[b]*Institute of Physics, Academy of Sciences of the Czech Republic, Na Slovance 2, 182 21 Praha 8, Czech Republic*

Received 1st November 2001, Accepted 29th November 2001
First published as an Advance Article on the web 21st March 2002

$K_{1.33}P_4W_8O_{32}$ belongs to the homologous series of monophosphate tungsten bronzes with hexagonal tunnels $A_x(PO_2)_4(WO_3)_{2m}$ with $0 < x < 2$ and $4 < m < 14$. $K_{1.33}P_4W_8O_{32}$ exhibits a phase transition at $T_c = 165$ K, that is characterized by an anomaly in the temperature dependence of the electrical resistivity and by the occurrence of extra reflections in the X-ray scattering. Here we report the $2a \times b \times c$ superstructure at $T = 120$ K, as it was measured by X-ray diffraction with synchrotron radiation. The superstructure is found to be monoclinic $P2_1$ with lattice parameters $a = 13.373(7)$ Å, $b = 5.3282(1)$ Å, $c = 8.926(4)$ Å, and $\beta = 100.65°$. The structure was refined within the superspace approach with superspace group $P2_1(\alpha, 0, \gamma)$ with $\alpha = 0.5$ and $\gamma = 0$. Final agreement was obtained at $R = 0.032$ ($R = 0.025$ for the main reflections and $R = 0.153$ for the superstructure reflections). The maximum shift out of the average position was 0.25 Å for one of the oxygen atoms. An analysis of the displacements and variations of interatomic distances is used to show that the mechanism of the phase transition is to resolve the internal strain between the K atoms and the surrounding PO_4 groups. The comparison with the CDW structure of $(PO_2)_4(WO_3)_{2m}$ shows that the phase transition is not a charge-density wave, but rather that the anomaly in the resistivity is caused by the changes in the structure when going through the phase transition.

1 Introduction

The phosphate tungsten bronzes comprise a large family of compounds showing a great variety of crystal structures. All of them are based on slabs of composition WO_3 with the ReO_3-type structure. The monophosphate tungsten bronzes $(PO_2)_4(WO_3)_{2m}$ with $2 \leqslant m \leqslant 14$ are built of slabs of corner-sharing WO_6 octahedra.[1] These slabs are connected through layers containing tetrahedral PO_4 groups and tunnels with a pentagonal shape: monophosphate tungsten bronzes with pentagonal tunnels, MPTBp (Fig. 1). The interest in these compounds derives from the fact that they are highly anisotropic low-dimensional electrical conductors, and that they show charge-density wave (CDW) transitions. Both the structures and the physical properties depend on m. In general, the transition temperatures (T_{CDW}) towards the low-temperature CDW state increase with m, while the width of the conducting slabs is proportional to m (ref. 2).

The tunnels in the phosphate bronzes can accommodate additional atoms, resulting in compounds with the general formula $A_x(PO_2)_4(WO_3)_{2m}$ with A = K, Na, Pb and $0 \leqslant x \leqslant 4$.[3–5] Direct intercalation into the pentagonal tunnels of the MPTBp has been found, but for most compositions the juxtaposition of the slabs in the intercalated compounds is different from that in the MPTBp, such that the intercalated atoms are accommodated in hexagonal tunnels: MPTBh (Fig. 2). Different packings of the slabs are found in compounds $A_x(PO_2)_4(WO_3)_{2m}$ with cations larger than K^+, *e.g.* A = Rb, Ba, corresponding to diphosphate tungsten bronzes with hexagonal tunnels (DPTBh). The intercalated compounds exhibit low-dimensional electronic properties, but otherwise their physical properties differ dramatically from those of the pristine compounds. With the exception of very small x ($x \leqslant 0.1$) the compounds with Na and Pb do not show phase transitions. The same is true for A = K and $m = 6$. Anomalies in the temperature dependence of the electrical resistivity have been found only for the compounds $K_x(PO_2)_4(WO_3)_8$.[6–8] The largest effect and a maximum transition temperature of $T_{CDW} = 170$ K have been found for $x = 1.30$. The phase transition is accompanied with the development of satellite reflections in the X-ray scattering. The commensurate wavevector $\boldsymbol{q} = 0.5\boldsymbol{a}^*$

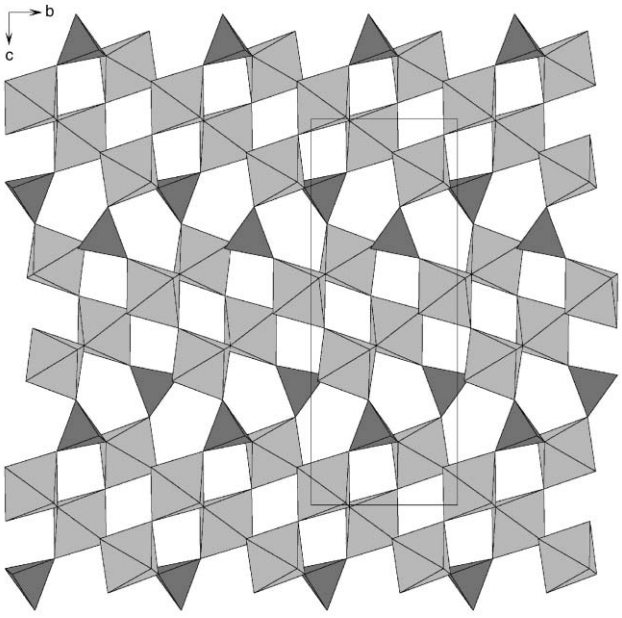

Fig. 1 View of the structure of $(PO_2)_4(WO_3)_8$[15] along $\boldsymbol{b}$ showing typical pseudo-pentagonal channels in this MPTBp. The WO_6 octahedra and PO_4 tetrahedra are indicated in light and dark grey, respectively.

 DOI: 10.1039/b109982p

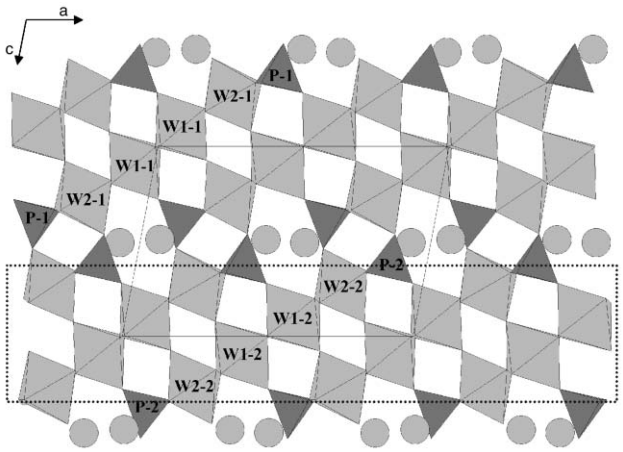

Fig. 2 View of the superstructure $K_{1.33}P_4W_8O_{32}$ along the monoclinic ***b*** axis. The WO_6 octahedra and PO_4 tetrahedra are indicated in light and dark grey, respectively. The atoms outside of polyhedra are potassium. The "-1" and "-2" identifiers in the atomic labels denote two independent parts of the superstructure. The dashed rectangle shows single conducting slab parallel with the ***ab*** plane and isolated from neighbouring slabs by PO_4 tetrahedra and potassium atoms.

is the same for all x.[7] It was concluded that the phase transitions in $K_x(PO_2)_4(WO_3)_8$ are not conventional Peierls instabilities as opposed to the transitions in the pristine compound $(PO_2)_4(WO_3)_8$.[1,2]

In the present work we report the 2-fold superstructure of $K_{1.33}(PO_2)_4(WO_3)_8$ as determined from single-crystal X-ray diffraction with synchrotron radiation at $T = 110$ K. A detailed analysis of the superstructure effects shows that the driving force for the phase transition in $K_{1.33}(PO_2)_4(WO_3)_8$ is not an instability in the electronic bands, but instead should be sought in a relaxation of the strain in the coordination polyhedra of the potassium atoms.

2 Experimental

Single crystalline material of $K_{1.33}(PO_2)_4(WO_3)_8$ was kindly donated by Groult and Labbé.[6] A single crystal of dimensions $0.01 \times 0.04 \times 0.03$ mm^3 was selected for the diffraction experiment. The large facets corresponded to the (001) and (00−1) crystal faces.

X-Ray diffraction at room temperature on a Nonius MACH3 4-circle diffractometer with rotating anode confirmed the crystal structure of this compound. The shape of the crystal was determined from the ψ-scans of 86 reflections using the computer program HABITUS.[9] This shape was used for absorption correction of the intensity data.

A low-temperature X-ray diffraction experiment was performed at beamline BM01 at the ESRF in Grenoble, France. The crystal was mounted on a KUMA six-circle diffractometer operating in four-circle mode. The crystal was kept at a temperature of $T = 110$ K using an Oxford Cryosystems nitrogen-gas flow cryostat. CCDC number 164462. See http://www.rsc.org/suppdata/jm/b1/b109982p/ for crystallographic files in .cif or other electronic format.

In addition to the strong Bragg reflections of the basic structure, weak superstructure reflections were observed at the expected positions corresponding to a $2a \times b \times c$ supercell. Even with the synchrotron radiation they appeared weak. From the total of 1445 measured reflections of this type 849 had an intensity less than 3σ and only 202 reflections were stronger than 10σ. The data reduction including the absorption correction using the optimized crystal shape, as well as all subsequent calculations, were made with the computer program JANA2000.[10] The experimental details are summarized in Table 1.

Table 1 Experimental data

Temperature/K	110
Chemical formula	$K_{1.33}P_4W_8O_{32}$
Z	1
M_r	2158.7
Crystal system	Monoclinic
Space group	$P2_1$ (No. 4)
a/Å	13.373(7)
b/Å	5.3282(11)
c/Å	8.926(4)
β/deg	100.65
D_c/g cm^{-3}	5.733
Crystal size/mm^3	0.04 × 0.03 × 0.01
Crystal color	Purple
Crystal form	Platelet
Diffractometer	Kuma 6 circles limited to 4 circles with point detector
Wave length λ/Å	0.5900 (synchrotron)
Scan mode	ω
Maximal theta/deg	22.80
Range of h, k, l	−17 to 17, 0 to 6, −11 to 10
Intensity decay (%)	4.9
Reflections for cell parameters	20 reflections between 15.2–33.6° θ
Absorption correction	Gaussian
Source of absorption coefficients	http://physics.nist.gov/cgi-bin/Xcom/xcom2
μ/cm^{-1}	227.8
Transmission factor T_{min}	0.4769
Transmission factor T_{max}	0.8020
No. of recorded reflections	2883
No. of independent reflections	1634
R_{int}	0.038
Criterion for observed reflections	$I > 2.5\sigma(I)$
No. of observed main reflections	789
No. of observed satellites	409
Refinement	on F
R^a for observed reflections	0.028
WR^a for observed reflections	0.060
S^a for all reflections	2.19
R^b for observed main reflections	0.025
R^b for observed satellites	0.153
No. of parameters in superstructure	217
No. of parameters in commensurate refinement	146
Weighting scheme	$w = 1/[\sigma^2(F) + 0.0004F^2]$
Extinction correction	Type 1, Lorentzian, isotropic
Extinction coefficient	0.26(3)
$(\Delta/\sigma)_{max}$	0.0005
$\Delta\rho_{max}$/e Å^{-3}	3.14
$\Delta\rho_{min}$/e Å^{-3}	−3.86
Scattering factor source	International Tables Vol. C
Source of f', f''	http://www-phys.llnl.gov/Research/scattering/asf.html

[a]Refinement in the supercell [b]superspace refinement.

3 Determination of the superstructure

3.1 Superspace approach to commensurate superstructures

For the structure solution and refinement we used the superspace approach.[11,12] The structure was described in the average unit cell and a modulation based on the commensurate wavevector $\boldsymbol{q} = 0.5\boldsymbol{a}^*$. Reflections were indexed with 4 integers (h, k, l, m) according to

$$\boldsymbol{H} = h\boldsymbol{a}^* + k\boldsymbol{b}^* + l\boldsymbol{c}^* + m\boldsymbol{q} \quad (1)$$

Main reflections correspond to (h, k, l, 0). Because of the commensurate value of the modulation wavevector only first-order satellites exist with indices (h, k, l, 1).

The atomic positions are given as the sum of an average position and a shift

$$x_i^\mu = \bar{x}_i^\mu + u_i^\mu(\bar{x}_{s4}), \quad (2)$$

Table 2 Possible supercell space groups for the different choices of the superspace group. The origin shifts as compared to the setting in the International Tables Vol. A are given in parentheses

Superspace group	$t = 0$	$t = ¼$	Other t
$P2_1/m(\alpha 0\gamma)$	$P2_1/m$	$P2_1/m(0,¼,0)$	$Pm(0,¼,0)$
$P2_1(\alpha 0\gamma)$	$P2_1$	$P2_1(¼,0,0)$	$P1$
$Pm(\alpha 0\gamma)$	$Pm(0,¼,0)$	$Pm(0,¼,0)$	$Pm(0,¼,0)$

$$\bar{x}_i^{\mu} = L_i + \bar{x}_i^{0\mu}, \tag{3}$$

$$\bar{x}_{s4} = t + \boldsymbol{q}\cdot\boldsymbol{x} \tag{4}$$

where $\bar{x}_i^{\mu}$ ($i = x, y, z$) are the coordinates of atom μ in the average structure with L_i integers and $\bar{x}_i^{0\mu}$ the average position within the unit cell. x_i^{μ} are the coordinates of the true position. The components of the modulation function of atom μ are $u_i^{\mu}(\bar{x}_{s4})$ with $u_i(\bar{x}_{s4} + 1) = u_i(\bar{x}_{s4})$. $\bar{x}_{s4} = t + \boldsymbol{q}\cdot\boldsymbol{x}$ is the fourth (superspace) coordinate with starting phase t.

The modulation functions for commensurate structures are only defined for points corresponding to translations of an average atomic position towards relevant positions in the supercell. For the present case a complete description of the superstructure is obtained with only one harmonic:

$$u_i^{\mu} = A_i^{\mu}\sin(2\pi\bar{x}_{s4}) + B_i^{\mu}\cos(2\pi\bar{x}_{s4}) \tag{5}$$

The structure depends on t, and there is only one value of t in the interval $<0, 0.5>$ that corresponds to the true structure. This value needs to be determined in the structure determination procedure.

3.2 Symmetry and structure refinements

The symmetry of a modulated structure can be expressed by a superspace group.[11] For an incommensurate structure this is the true symmetry. For a commensurate modulation the space group of the supercell can be derived from the superspace group in a unique way. Usually different space groups are obtained for different values for t. From this fact an important advantage of commensurate refinement arises: that different superstructure symmetries can be tested with the same average structure simply by changing t. Another benefit of using the modulated structure approach is that the displacements responsible for the superstructure can easily be found by refinement starting with arbitrary small values for the modulation parameters.

The systematic extinctions of main reflections (h, k, l, 0) indicated the existence of a two-fold screw axis along $\boldsymbol{b}$. The refinement of the average structure using the space group $P2_1/m$ converged to $R_F = 0.025$. This establishes that the room-temperature structure is retained as the average structure within the modulated phase in very good approximation.

Only superspace groups for the modulated structure were considered that are compatible with the $P2_1/m$ symmetry of the basic structure. Two centrosymmetric possibilities exist: $P2_1/m(\alpha 0\gamma)$ and $P2_1/m(\alpha 0\gamma)0s$, in both cases with $\alpha = 0.5$ and $\gamma = 0$. The latter superspace group was in contradiction with the systematic extinctions of the satellites and was thus discarded. Depending on the value of t, $P2_1/m(\alpha 0\gamma)$ leads to $P2_1/m$ or Pm as the space group of the supercell (Table 2). However, for both choices for the value of t we did not get satisfactory fits to the satellite reflections, with partial R factors of about 0.3. The refinement with the non-centrosymmetric superspace group $Pm(\alpha 0\gamma)$ was unstable and yielded unsatisfactory fits too.

The best fit to the data was obtained with the superspace group $P2_1(\alpha 0\gamma)$ and $t = ¼$. All refinements have been performed against the complete data including observed reflections and less than's. A smooth convergence was obtained to $R = 0.032$ for all reflections ($R = 0.025$ for observed main reflections and $R = 0.153$ for observed satellites). The value of $t = ¼$ corresponded to the space group $P2_1$ for the supercell. The number of independent atoms in this supercell is twice the number of independent atoms in the basic structure. Within the modulated structure approach this is fully described by using either the sine or the cosine amplitudes of the first harmonic modulation functions (eqn. (5)). We have used the sine components except for the atom O1 for which the cosine amplitudes were used. The average position of O1 is ($\sim$½, $\sim$0, $\sim$0) leading to values $\bar{x}_{s4} = 0.25 + \boldsymbol{q}\cdot\boldsymbol{x}^{01}$ approximately equal to zero, and resulting in sin ($\bar{x}_{s4}$) = $\approx$0. The relatively high value of the partial R-factor for the satellites is explained in part by the many satellite reflections that are close to the limit of observability. For example there are 95 satellites with $2.5\ \sigma(I) < I < 4\sigma(I)$. The expected R-value for $I = 4\sigma(I)$ reflections is 0.125.

The results of the superspace refinement are summarized in Table 3.

The temperature parameters represented a problematic part of the refinement, because they were not positive definite for all atoms. We have carefully checked the data reduction process (standard reflections decay, LP and absorption corrections) without finding any indication for errors or obvious inconsistencies. The measurement was done with continuous scan mode so that narrow peaks of low angle reflections could not cause the problem, too. The temperature of 110 K was large enough for sizable temperature factors being present. It must be concluded that the temperature parameters are negative for unknown reasons. The effect of the temperature factors on the structure model was analysed by additional refinements with positive temperature factors. With values of zero or 0.01 Å^2 or 0.1 Å^2 for the isotropic temperature factors of all atoms, convergence was attained at $R = 0.033$, $R = 0.037$ and $R = 0.085$ respectively. However, the differences between the values of the positional parameters in the original refinement and their values in the refinements with the positive isotropic

Table 3 Fractional atomic coordinates (x^0, y^0, z^0) and modulation parameters in Å (eqn. (5)) for the final superspace refinement. For O1 the modulation parameters refer to $B_{1,i}$, for the other atoms they refer to $A_{1,i}$. Standard deviations are given in parentheses

	x^0	y^0	z^0	A_{1x}/B_{1x}	A_{1y}/B_{1y}	A_{1z}/B_{1z}
W1	0.36129(4)	0.25	0.08793(3)	−0.0030(14)	0.0492(8)	0.0050(14)
O1	0.512(3)	0.009(4)	−0.007(2)	−0.060(8)	−0.048(6)	0.001(9)
O2	0.5738(11)	0.272(4)	0.2796(10)	0.066(45)	−0.207(24)	0.012(44)
W2	0.06469(5)	0.7510(4)	0.24865(4)	−0.0024(6)	0.0205(4)	0.0081(6)
O3	0.2077(19)	−0.002(3)	0.1820(15)	0.165(12)	−0.131(13)	0.035(11)
O4	0.2252(17)	0.507(2)	0.1942(17)	0.017(9)	0.027(10)	0.002(12)
O5	0.1340(9)	0.259(2)	−0.0762(6)	0.107(10)	−0.041(9)	0.018(11)
P	0.7909(3)	0.249(2)	0.3709(3)	0.003(5)	0.040(2)	0.018(5)
O6	0.7629(9)	0.262(3)	0.5380(8)	0.079(13)	0.038(8)	0.003(14)
O7	0.8967(16)	0.483(2)	0.3341(11)	−0.152(10)	0.149(9)	−0.012(8)
O8	0.9021(19)	0.009(2)	0.3395(19)	0.023(9)	0.026(10)	−0.022(12)
K	0.3638(8)	0.255(3)	0.5018(7)	0.020(24)	−0.113(14)	0.167(24)

temperature factors was always less than two times their respective standard deviations. Because the values of the superstructure shifts vary between 50σ (W atoms) and 10 to 20σ (other atoms), these values have been determined reliably despite the problems with the temperature factors. Furthermore, it is noted that this feature was present both for the refinement of the average structure against main reflections and for the complete structure refinement. Thus the problems with the temperature parameters are not caused by a wrong model for the shifts of the atoms in the superstructure. Because of the problems with negative temperature parameters we have refrained from an interpretation of their values and from a refinement of modulation functions for the temperature factors. Therefore the structure model ignores possible differences between temperature parameters of corresponding atoms at the two supercell positions, which is one reason for relatively high R values for satellite reflections. (The other reason is that the satellite reflections were weak.)

The final superspace structure model was transformed into the 3-dimensional supercell. Refinement of all independent parameters as allowed by the supercell symmetry $P2_1$ resulted in a fit with $R = 0.028$ for all observed reflections. This value is slightly lower than the one obtained with superspace refinement, as it is explained by the fact that now independent parameters for all atoms in the supercell were used. The fit to the main reflections was virtually the same as in the superspace refinement, but the fit to the satellites improved significantly to $R = 0.101$. The parameters of the supercell refinement are given in Table 4.

4 Discussion

4.1 Validation of the structure model

The space group $P2_1$ for the superstructure is non-centrosymmetric, and the absolute structure should be determined based on the anomalous dispersion coefficients. Refinement of the inversion-twin domain parameter resulted in a value of almost ½ without any significant lowering of the R value. Therefore it can be concluded that both configurations are present in equal amounts, in accordance with the expectations for a phase transition from a centrosymmetric towards an acentric structure.

The refined composition of potassium is $x = 1.32(1)$, in accordance with the nominal value of 4/3. The refinement and the Fourier maps confirmed that potassium is distributed statistically over the two independent atomic sites. There is no indication for a smearing of the density along the channels. In the commensurate refinement we refined the occupation of the single K-position without a modulation function. In the supercell two independent K-positions exist. The supercell refinement confirmed that these two positions have the same average occupancy.

Table 4 Fractional atomic coordinates and equivalent isotropic temperature parameters (Å^2) for the final refinement in the superstructure. Atoms are numbered according to the basic structure (Table 3) with the number following the dash indicating the two positions in the superstructure

Atom	Occupation	x	y	z	U_{eq}[a]
W1-1	1	−0.06944(5)	0.253898	0.08820(7)	−0.0024(3)
W1-2	1	0.43070(4)	0.24604(16)	0.08763(7)	−0.0035(2)
O1-1	1	0.007(2)	0.025(5)	−0.004(3)	0.007(4)
O1-2	1	0.499(2)	0.006(5)	−0.004(3)	−0.003(3)
O2-1	1	0.0365(11)	0.283(4)	0.2789(16)	0.004(4)
O2-2	1	0.5380(8)	0.263(4)	0.2787(14)	−0.005(3)
W2-1	1	−0.21773(5)	0.7545(4)	0.24932(7)	−0.0029(3)
W2-2	1	0.28242(5)	0.7472(3)	0.24799(7)	−0.0032(2)
O3-1	1	−0.1377(19)	−0.018(5)	0.180(2)	0.014(6)
O3-2	1	0.3433(13)	0.020(4)	0.176(2)	−0.001(4)
O4-1	1	−0.1364(12)	0.511(3)	0.198(2)	−0.005(4)
O4-2	1	0.3627(12)	0.509(3)	0.1986(17)	−0.016(3)
O5-1	1	−0.1764(8)	0.262(6)	−0.0746(12)	0.001(4)
O5-2	1	0.3103(8)	0.271(4)	−0.0779(13)	−0.003(3)
P-2	1	0.1454(3)	0.244(2)	0.3708(5)	−0.0002(13)
P-1	1	0.6454(3)	0.257(2)	0.3711(4)	−0.0044(11)
O6-1	1	0.1282(8)	0.256(3)	0.5369(15)	0.002(3)
O6-2	1	0.6347(9)	0.266(4)	0.5389(11)	0.004(3)
O7-1	1	0.2072(15)	0.458(4)	0.3360(17)	0.005(5)
O7-2	1	0.6850(12)	0.516(3)	0.3339(16)	−0.006(3)
O8-1	1	0.2017(12)	0.010(3)	0.343(2)	0.002(4)
O8-2	1	0.7056(12)	0.019(3)	0.334(2)	−0.001(4)
K-1[b]	0.327	−0.0678(8)	0.246(3)	0.5087(12)	0.001(3)
K-2[b]	0.327	0.4322(8)	0.266(4)	0.4925(15)	0.014(4)

[a] $U_{eq} = \frac{1}{3}\sum_{i=1}^{3}\sum_{j=1}^{3} U^{ij} a_i^* a_j^* a_i a_j$ [b] Statistical occupation 0.327(10).

4.2 The possibility of a CDW

The largest displacement of a tungsten atom from the average position is 0.025(2) Å for W2-1. The displacements are mainly along ***b*** (Table 5). Despite their low values, the displacements of the tungsten atoms were very important for arriving at a good fit to the data, and their values appear as highly significant (Tables 3 and 4). The influence of these displacements on the W–W distances within one particular WO_3 slab is displayed in Fig. 3 and in Table 6. The network of short distances remains the same as in the average structure, whereby the shortest distances are even shorter in the superstructure. A pronounced feature of the superstructure is the mutual shift of parts of the slabs in the ***b*** direction as indicated in Fig. 3.

In Table 6 the tungsten–tungsten distances in the superstructure are compared with those in the average structure. The maximal change is 0.01 Å which is much less than the potential maximal value 0.10 Å resulting from the maximal displacement of tungsten from the average position. The displacement of tungsten from the average positions is virtually not projected into the bond lengths changes, which is a strong argument that the electronic instabilities in this compound are not caused by forming a CDW. Moreover, this argument can be supported by a different behavior of the parent $(PO_2)_4(WO_3)_8$ compound, where a 2-dimensional CDW has been characterized.[13] In this compound the maximal displacements of tungsten and variations of W–W bond lengths of up to 0.04 Å were observed.[14,15] The values are larger than presently found for $K_{1.33}P_4W_8O_{32}$, despite the fact that the transitions in the pristine compound are at much lower temperatures.

4.3 A strain driven transition

In the average structure W–O distances (Å) range from 1.8760(2) to 2.020(7) Å for W1 ($\Delta = 0.144$ Å) and from 1.804(4) to 2.043(6) Å for W2 ($\Delta = 0.239$ Å). The angles in the WO_6 octahedra deviate from the ideal value of 90° by

Table 5 Positions of tungsten in the average structure and in the superstructure of $K_{1.33}P_4W_8O_{32}$. The symbols Δ_x, Δ_y, Δ_z and Δ represent the distances between positions of the same atom in the average structure and the superstructure in the x, y, z directions and in the connection direction, respectively. The average fractional coordinates are transformed to the supercell

Atom name	x_{aver} x_{sup}	y_{aver} y_{sup}	z_{aver} z_{sup}	Δ_x/Å	Δ_y/Å	Δ_z/Å
W1-1	−0.06936	0.25000	0.08791	0.001	0.020	0.002
	−0.06943	0.25390	0.08820			
W1-2	0.43064	0.25000	0.08791	0.0	0.021	0.002
	0.43070	0.24604	0.08763			
W2-1	−0.21767	0.75000	0.24864	0.0	0.024	0.006
	−0.21773	0.75451	0.24932			
W2-2	0.28233	0.75000	0.24864	0.001	0.014	0.005
	0.28242	0.74722	0.24799			

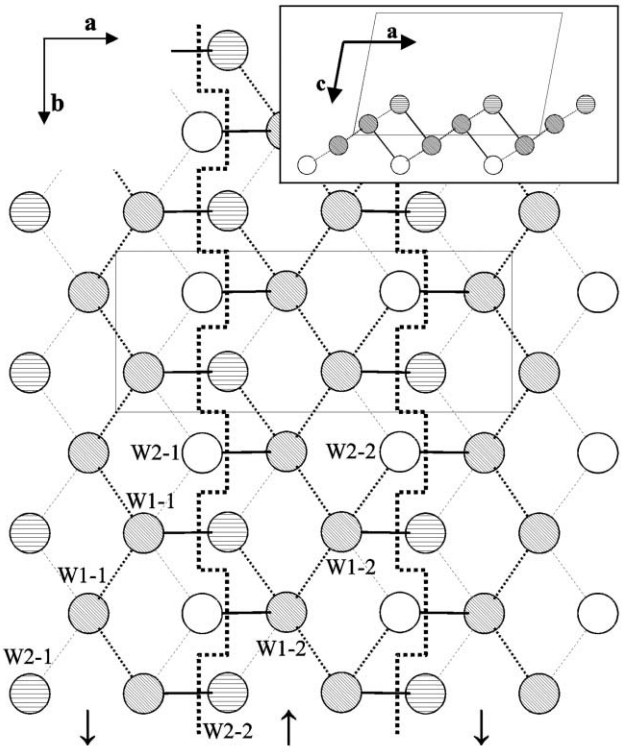

Fig. 3 Single slab of tungsten atoms in the superstructure viewed along the negative direction of ***c***. A dense hatching represents atoms in the middle of the slab, the atoms above them are clear and the ones below are hatched horizontally. The parts of the slab separated by a thick dashed line are shifted as indicated by the arrows in the bottom. The distances between tungsten atoms are sorted as follows: the thick solid lines represent the bond lengths 3.736 and 3.741 Å (3.738 Å in the average structure); the thick dashed lines represent the bond lengths 3.749 and 3.754 Å (3.751 Å in the average structure); the thin dashed lines represent bond lengths 3.756, 3.760, 3.763 and 3.764 Å (3.760 in the average structure). In the insert the same atoms are plotted in a view along ***b***.

maximally 5.4° for W2. The distances P–O within the PO_4 tetrahedra are between 1.511(6) and 1.532(7) Å, much closer to the ideal value (Δ = 0.021 Å). However, the deviation of angles from the ideal tetrahedral value is 5.4°, which is comparable to the deviations found for WO_6.

In the superstructure the values of the W–O and P–O bond lengths and their variations (Table 7) are similar to the values and variations found in the average structure. The bond angles deviate much more from their ideal values within the superstructure, reaching 9.3° for the octahedron of W1-1, 7.8° for that of W1-2, 10° for that of W2-1, and 13° for the octahedron of W2-2. Maximum deviations are 8.6° for the tetrahedron of P-1 and 9.1° for the tetrahedron of P-2.

Table 6 Distances between tungsten atoms (Å) for the average structure and for the superstructure of $K_{1.33}P_4W_8O_{32}$. In the last column there are the differences between the shortest and longest W–W distance pertaining to the relevant distance in the average structure. The numbers are rounded to three decimal digits that are significant in all cases

Atoms	Average structure	Superstructure	Δ/Å
W1-1^{i}–W2-2^{ii}	3.738	3.736	0.005
W1-2^{i}–W2-1^{ii}	3.738	3.741	
W1-2^{i}–W1-2^{iii,vi}	3.752	3.749	0.007
W1-1^{i}–W1-1^{ii,v}	3.752	3.756	
W1-2^{i}–W2-2^{iv}	3.760	3.754	0.010
W1-1^{i}–W2-1^{iv}	3.760	3.760	
W1-2^{i}–W2-2^{i}	3.760	3.763	
W2-1^{i}–W1-1^{i}	3.760	3.764	

Symmetry codes: (i) x,y,z; (ii) $-x,-\frac{1}{2}+y,-z$; (iii) $1-x,\frac{1}{2}+y,-z$; (iv) $x,-1+y,z$; (v) $-x,\frac{1}{2}+y,-z$; (vi) $1-x,-\frac{1}{2}+y,-z$

Table 7 Distances (Å) and angles (°) within the WO_6 octahedra and within the PO_4 tetrahedra. Only the angles are listed which differ more than 2.5° from the ideal value 90° for WO_6 and 109.4° for PO_4, respectively

Atoms	*d*/angle	Atoms	*d*/angle
W1-1–O1-1	1.88(3)	W2-2–O3-2^{iii}	1.84(2)
W1-1–O1-1^{i}	1.89(3)	W2-2–O4-2	1.770(16)
W1-1–O2-1	2.009(13)	W2-2–O5-1^{i}	1.898(10)
W1-1–O3-1	1.97(2)	W2-2–O6-2^{vii}	2.020(9)
W1-1–O4-1	1.99(2)	W2-2–O7-1	2.07(2)
W1-1–O5-1	1.841(10)	W2-2–O8-1^{iii}	2.05(2)
O1-1–W1-1–O2-1	93.9(10)	O3-2^{iii}–W2-2–O4-2	98.7(8)
O1-1–W1-1–O5-1	94.3(11)	O3-2^{iii}–W2-2–O6-2^{vii}	95.1(8)
O1-1^{i}–W1-1–O4-1	86.7(11)	O3-2^{iii}–W2-2–O8-1^{iii}	84.7(8)
O2-1–W1-1–O4-1	80.7(7)	O4-2–W2-2–O5-1^{i}	102.9(9)
W1-2–O1-2	1.85(2)	O4-2–W2-2–O7-1	85.4(8)
W1-2–O1-2^{ii}	1.90(2)	O5-1^{i}–W2-2–O8-1^{iii}	86.5(8)
W1-2–O2-2	2.018(10)	O6-2^{vii}–W2-2–O7-1	84.3(7)
W1-2–O3-2	1.94(2)	O6-2^{vii}–W2-2–O8-1^{iii}	79.2(7)
W1-2–O4-2	2.026(16)	P-1–O2-2	1.518(10)
W1-2–O5-2	1.978(10)	P-1–O6-2	1.531(11)
O1-2–W1-2–O2-2	94.1(9)	P-1–O7-2	1.54(2)
O1-2–W1-2–O5-2	96.7(9)	P-1–O8-2	1.57(2)
O1-2^{ii}–W1-2–O5-2	92.9(9)	O2-2–P-1–O6-2	106.3(7)
O2-2–W1-2–O3-2	94.2(7)	O2-2–P-1–O7-2	101.1(11)
O2-2–W1-2–O4-2	82.5(6)	O2-2–P-1–O8-2	112.0(11)
O3-2–W1-2–O4-2	82.7(8)	O6-2–P-1–O7-2	106.2(12)
O3-2–W1-2–O5-2	82.9(7)	O6-2–P-1–O8-2	112.1(11)
O4-2–W1-2–O5-2	86.7(6)	O7-2–P-1–O8-2	118.0(9)
W2-1–O3-1^{iii}	1.80(2)	P-2–O2-1	1.548(15)
W2-1–O4-1	1.804(19)	P-2–O6-1	1.543(15)
W2-1–O5-2^{i}	1.783(10)	P-2–O7-1	1.47(2)
W2-1–O6-1^{iv}	2.056(12)	P-2–O8-1	1.50(2)
W2-1–O7-2^{v}	2.060(18)	O2-1–P-2–O6-1	102.2(7)
W2-1–O8-2^{vi}	1.977(18)	O2-1–P-2–O8-1	118.5(11)
O4-1–W2-1–O5-2^{i}	100.0(8)	O7-1–P-2–O8-1	106.8(11)
O4-1–W2-1–O7-2^{v}	95.7(8)		
O6-1^{iv}–W2-1–O8-2^{vi}	84.0(6)		
O7-2^{v}–W2-1–O8-2^{vi}	83.8(7)		

Symmetry codes:(i) $-x,\frac{1}{2}+y,-z$; (ii) $1-x,\frac{1}{2}+y,-z$; (iii) $x,1+y,z$; (iv) $-x,\frac{1}{2}+y,1-z$; (v) $x-1,y,z$; (vi) $x-1,1+y,z$; (vii) $1-x,\frac{1}{2}+y,1-z$

Fig. 4 compares positions of atoms in two sections of the slabs corresponding to the two configurations that are present in the superstructure. The major shifts are found for potassium and especially oxygen atoms (Table 8). Fig. 4 suggests that the displacements of the oxygen atoms are smaller towards the centers of the slabs. However, the maximum displacements in this area are in the direction perpendicular to the plane of the drawing. The basic structure contains one symmetry independent potassium atom. In the superstructure there are two independent potassium atoms that have considerably different coordinations (Table 9). Both the shifts of the potassium atoms and the displacements of the oxygen atoms are responsible for this variation. Because the shortest K–O distances concern oxygen atoms of the PO_4 tetrahedra, the question arises whether the generation of more stable environments of K and P might be the driving force for the phase transition.

Indeed, as demonstrated in Fig. 5(a), the PO_4 tetrahedron oscillates between two positions minimizing different K–O distances. The corresponding movement is a combination of a rotation and an angle deformation. In the configuration indicated in Fig. 5(a) by large circles for the oxygen atoms the distance K–O8 is minimized and the angle O2–P–O8 = 119° is the most deformed one in the PO_4 tetrahedron. The second configuration with oxygen atoms at the positions of the small filled circles, the distance K–O7 is the minimal one, and the angle deformation concentrates in O7–P–O8 = 118°. Fig. 5(b) shows the PO_4 neighborhood for the centrosymmetric average structure. Here the K–O8 and K–O7 distances are the

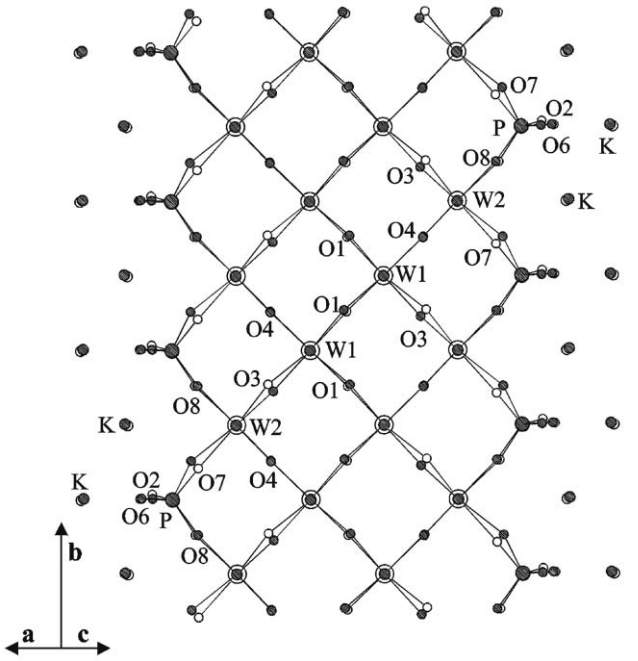

Fig. 4 Superposition of two sections (indicated in Fig. 2 by labelled atoms) of WO_3-type slab in $K_{1.33}P_4W_8O_{32}$. The sections correspond to the two possible configurations occurring in the superstructure. The picture is rotated to get the maximum overlap of two planes of tungsten atoms. The off plane oxygen atoms O2, O5 and O6 are omitted.

Table 8 Shifts in Å between atomic positions in the average structure and in the superstructure (Δ_{av}) and the sum of the shifts pertaining two positions of an atom in the superstructure (Δ_{tot}). The numbers are rounded to a hundredth of an angstrom and sorted in ascending order

Atom	Δ_{av}	Atom	Δ_{av}	Atom	Δ_{tot}
W1-1	0.02	O4-2	0.10	W1	0.04
W1-2	0.02	O6-2	0.10	W2	0.05
W2-2	0.02	O4-1	0.11	P	0.07
W2-1	0.03	O5-1	0.11	O6	0.15
P-2	0.03	O3-1	0.12	O8	0.15
P-1	0.04	K-2	0.12	K	0.19
O1-2	0.05	O5-2	0.14	O4	0.21
O6-1	0.05	O1-1	0.17	O1	0.22
O8-1	0.06	O2-1	0.18	O2	0.25
O2-2	0.07	O7-1	0.18	O5	0.25
K-1	0.07	O3-2	0.25	O3	0.37
O8-2	0.09	O7-2	0.25	O7	0.43

Table 9 Coordination of potassium calculated up to 3.5 Å. In the left column the distances pertaining to K-1 coordination are sorted in ascending order. The right column contains corresponding distances to K-2

Atoms	*d*/Å	Atoms	*d*/Å
K-1–O6-1	2.59(2)	K-2–O6-2	2.66(2)
K-1–O2-1	2.69(2)	K-2–O2-2	2.58(2)
K-1–O6-1^{I}	2.75(2)	K-2–O6-2^{iv}	2.80(3)
K-1–O8-1^{ii}	2.79(2)	K-2–O8-2^{v}	2.94(2)
K-1–O6-1^{ii}	2.84(2)	K-2–O6-2^{v}	2.81(3)
K-1–O7-1^{I}	2.95(2)	K-2–O7-2^{iv}	2.74(2)
K-1–O2-1^{I}	3.09(2)	K-2–O2-2^{iv}	3.35(3)
K-1–O4-1	3.09(2)	K-2–O4-2	2.92(2)
K-1–P-2^{ii}	3.11(2)	K-2–P-1^{v}	3.14(2)
K-1–P-2^{i}	3.13(2)	K-2–P-1^{iv}	3.22(2)
K-1–O3-1	3.23(2)	K-2–O3-2	3.14(2)
K-1–P-2	3.31(1)	K-2–P-1	3.23(1)
K-1–K-1^{I}	3.24(2)	K-2–K-2^{iv}	3.21(2)
K-1–K-1^{ii}	3.24(2)	K-2–K-2^{v}	3.21(2)
K-1–O8-2^{iii}	3.37(2)	K-2–O8-1	3.41(2)
K-1–O2-1^{ii}	3.41(2)	K-2–O2-2^{v}	3.32(2)
(K-1–O7-2)	3.68(2)	K-2–O7-1	3.24(2)

Symmetry codes: (i) $-x,y-\frac{1}{2},1-z$; (ii) $-x,\frac{1}{2}+y,1-z$; (iii) $x-1,y,z$; (iv) $1-x,y-\frac{1}{2},1-z$; (v) $1-x,\frac{1}{2}+y,1-z$

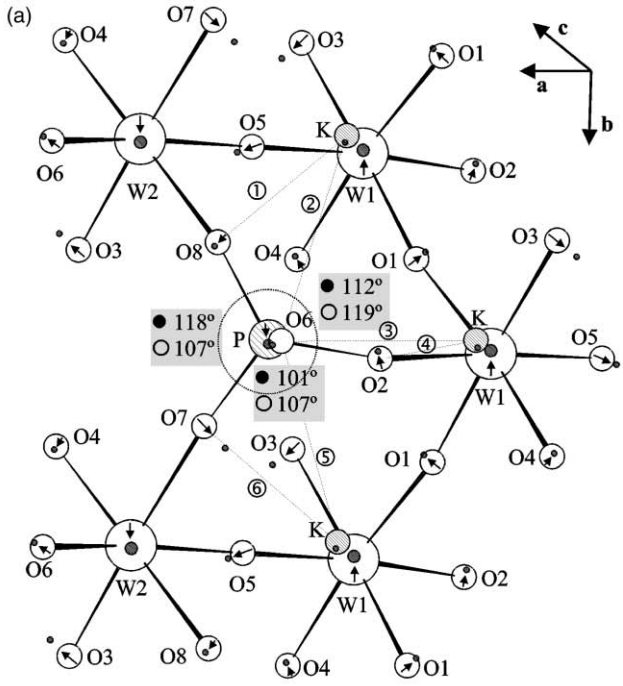

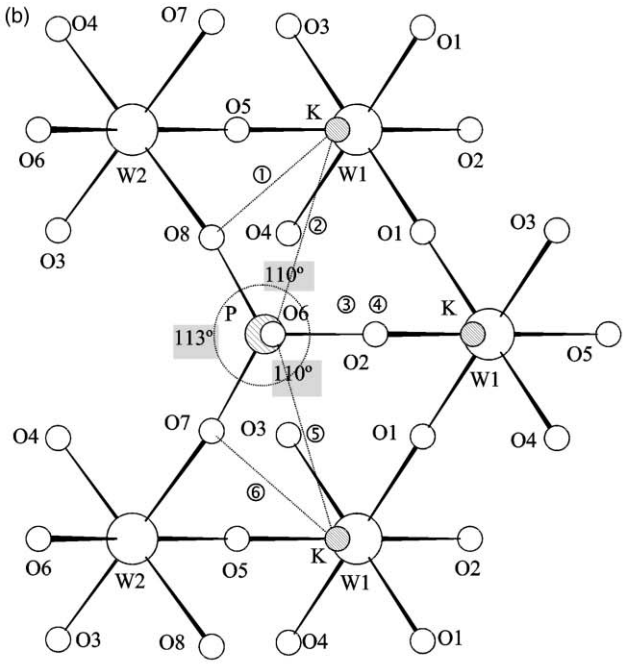

Fig. 5 The neighbourhood of PO_4 tetrahedron in a view perpendicular to the plane defined by O2, O7 and O8. The dotted lines represent the shortest K–O interactions. The angles given for PO_4 are rounded to full degrees. (a) Overlap of two configurations in the superstructure. The large open circles and the small filled circles represent the first and the second configuration, respectively. Arrows indicate the transition between both configurations. (b) The same area in the centrosymmetric average structure. Atoms have the same labels as in the superstructure.

same because O7 and O8 are symmetrically equivalent and the discussed angles reach almost ideal values.

Because PO_4 and WO_6 polyhedra share oxygen atoms, the displacement of the PO_4 tetrahedron causes corresponding displacement of WO_6 octahedra. This movement cannot be described as a rotation (see atom pairs O1 and O4 or O4 and O6 in Fig. 5(a)). The displacement of WO_6 finally results in small displacements of tungsten along ***b*** that can be therefore directly derived from the PO_4 movement. For instance, O2 moves up causing the displacement of neighboring W1 in the same direction. The same relation exists between pairs O8–W2 and O7–W2, respectively. The atoms W1 and W2 belong to the parts of WO_3-type slab displaced in the antiphase (Fig. 3).

5 Conclusions

We have determined the 2-fold superstructure of $K_{1.33}P_4W_8O_{32}$ as it exists below the phase transition at $T_c = 165$ K. Two mechanisms can be envisaged for the phase transition. In the first one the displacements originate in PO_4 tetrahedra oscillation between two positions within the framework of potassium atoms. This gives rise to displacement of oxygen, potassium, phosphorus and to a lesser extent of tungsten, too. The content of potassium influences the strength of the PO_4–K interactions and indirectly the tungsten positions. The second mechanism is that the primary force is an instability in the conduction bands, *i.e.* formation of a CDW. The changes in tungsten positions could break the equilibrium between positions of PO_4 and potassium causing oscillation of tetrahedra.

We found strong arguments against the second interpretation based on tungsten–tungsten distances, which do not reflect the changes in tungsten positions. Therefore, we conclude that the phase transition in $K_x(PO_2)_4(WO_3)_8$ is a strain driven transition originating in the forces between potassium and the PO_4 tetrahedra. This implies that an instability in the valence bands is not the origin of the phase transition. The anomaly in the electronic conductivity that was observed at T_c should then be ascribed to changes in the electronic band structure at this temperature.

Acknowledgement

The crystals were kindly donated by D. Groult. We thank S. Capilli and P. Pattison from ESFR for assistance with the synchrotron experiment. Beam-time at Beam line BM01 of the ESRF was obtained under general user proposal HS-1111. Financial support by the German Science Foundation (DFG) and the FCI as well as under grant Number 202/00/0645 of the Grant agency of the Czech Republic is gratefully acknowledged.

References

1 P. Roussel, P. Labbé and D. Groult, *Acta Crystallogr., Sect. B*, 2000, **B56**, 377.
2 A. Ottolenghi and H.-P. Pouget, *J. Phys. I*, 1996, **6**, 1059.
3 J. P. Giroult, M. Goreaud, P. Labbé and B. Raveau, *J. Solid State Chem.*, 1982, **44**, 407.
4 P. Roussel, D. Groult, A. Maignan and P. Labbé, *Chem. Mater*, 1999, **11**, 2049.
5 P. Roussel, A. C. Masset, B. Domenges, A. Maignan, D. Groult and P. Labbé, *J. Solid State Chem.*, 1998, **139**, 362.
6 P. Roussel, D. Groult, C. Hess, P. Labbé and C. Schlenker, *J. Phys. Condens. Matter*, 1997, **9**, 7081.
7 J. Dumas, U. Beierlein, S. Drouard, C. Hess, D. Groult, P. Labbé, P. Roussel, G. Bonfait, E. G. Marin and C. Schlenker, *J. Solid State Chem.*, 1999, **147**, 320.
8 S. Drouard, D. Groult, J. Dumas, R. Buder and C. Schlenker, *Eur. Phys. J. B*, 2000, **16**, 593.
9 W. Herrendorf, PhD Thesis, University of Karlsruhe, Germany, 1992.
10 V. Petricek and M. Dusek, The crystallographic computing system JANA2000, Institute of Physics, Praha, Czech Republic, 2000.
11 P. M. de Wolff, T. Janssen and A. Janner, *Acta Crystallogr., Sect. A*, 1981, **37**, 625.
12 S. van Smaalen, *Crystallogr. Rev.*, 1995, **4**, 79.
13 P. Roussel, S. Drouard, D. Groult, P. Labbé, J. Dumas and C. Schlenker, *J. Mater. Chem.*, 1999, **9**, 973.
14 J. Ludecke, A. Jobst and S. van Smaalen, *Europhys. Lett.*, 2000, **49**, 357.
15 J. Lüdecke, A. Jobst, S. Geupel and S. van Smaalen, *Phys. Rev. B*, 2001, **64**, 104105.